IEEE International Conference on Ultra-Wideband, 5-8 Sept. 2005 Page(s):16 - 21

Propagation Effects in UWB Body Area Networks

Thomas Zasowski, Gabriel Meyer, Frank Althaus, and Armin Wittneben

Swiss Federal Institute of Technology (ETH) Zurich
Communication Technology Laboratory, Sternwartstrasse 7, 8092 Zurich, Switzerland
Email: zasowski@nari.ee.ethz.ch

***Abstract*— Due to the ongoing miniaturization of electronic devices and due to a multitude of applications, *wireless body area networks* (WBANs) have gained much interest recently. *Ultra wideband* (UWB) communication is one promising transmission technology for WBANs due to reduced hardware complexity. To optimize receiver structures and antennas for UWB WBANs it is necessary to know the propagation mechanisms at the human body. In this paper, we focus on transmission at the head and consider *direct transmission*, *surface waves*, *reflections*, and *diffraction* as possible propagation mechanisms in the frequency range between 1.5-8 GHz. We show theoretically and by measurement results that the direct path is attenuated such that direct transmission through the head is negligible. Based on measurements we conclude by process of elimination that diffraction is the main propagation mechanism around the human body and that surface waves and reflections are negligible. Finally, we discuss the impact of the propagation mechanisms on the UWB WBAN communication system.**

I. Introduction

Trends and technical developments of the last few years are pointing toward several promising applications for *wireless body area networks* (WBANs) such as health monitoring or ubiquitous computing [1]–[3]. Therefore, WBANs attracted increasing attention recently. In a WBAN, several small nodes are placed close or directly on the human body. Since such nodes shall get their power from rechargeable batteries or by energy harvesting they have to be very energy efficient [4]. Moreover, due to cost reasons and due to the relative high number of nodes in a WBAN the nodes shall be of low complexity.

One transmission technology for WBANs promising less complex hardware is *ultra wideband* (UWB) communication [5]. There, transmission takes place in baseband, i.e., no hardware is required for mixers, RF oscillators or PLLs, as it would be necessary in narrowband systems [6]. For optimization of UWB WBANs propagation effects on the body have to be known. Therefore, we perform measurements of the UWB WBAN channel in the frequency range from 1.5-8 GHz. In this contribution, we concentrate on propagation effects to be considered for antennas mounted on opposite sides of the head. Due to the proximity of the most important human communication organs, as e.g. mouth, eyes, and ears, the head is very attractive for the placement of transmitter and receiver. Moreover, effects from varying positions of extremities are reduced for such a scenario. Since only propagation effects around the human body shall be determined and not any effects caused by echoes from the environment, measurements are done in an anechoic chamber with several test persons and for reproducibility reasons also with a head phantom.

Up to now, there exist only few investigations of the UWB BAN channel. The impact of the body on UWB transmission was investigated in [7]. But there, only one antenna was mounted directly on the body and transmission between two antennas placed directly on the body was not considered. In [8], channel measurements were performed from 3-6 GHz on the front side of the body and around the torso. Main channel parameters, as e.g., path loss, delay spread and mean excess delay were extracted. But it was not distinguished between different propagation mechanisms. Another investigation of the UWB BAN channel from 3-6 GHz was presented in [9]. There, measurements were performed in an indoor environment to achieve realistic propagation conditions. It was shown that frequency correlation properties of the channel change significantly and significant variations of signal energy spread in time-delay domain were observed. But different propagation mechanisms around the human body were not investigated, too. In [10], WBAN channel parameters were derived by means of *Finite Difference Time Domain* (FDTD) simulations in the frequency range from 2-6 GHz showing that no direct transmission through the head takes place.

In Section II the measurement setup is described. The attenuation on the human head without considering different propagation mechanisms is presented in Section III. Keeping this expected attenuation on the human head in mind, in Section IV dominant propagation mechanisms are determined by process of elimination based on measurements and calculations. The impact of these results on UWB WBAN communication systems is discussed in Section V. Conclusions are drawn in Section VI.

II. Measurement Setup

Channel measurements were performed with a vector network analyzer (VNA) in the frequency range from $1.5-8$GHz using Skycross SMT-3TO10M-A antennas. To reduce the influence of unwanted cable effects on the measurements the antennas were mounted on *glass-fiber reinforced plastic* (GRP) arms on tripods as shown in Fig. 1. The tripods were covered by absorbing material to reduce reflections caused by them. With such a measurement setup only the antennas were placed close to the head while the cables led away from head as fast as possible.

Measurements were performed with 4 different test persons and for reproducibility reasons also with a SAM head phantom V4.5 from SPEAG [11]. The phantom was filled with the head

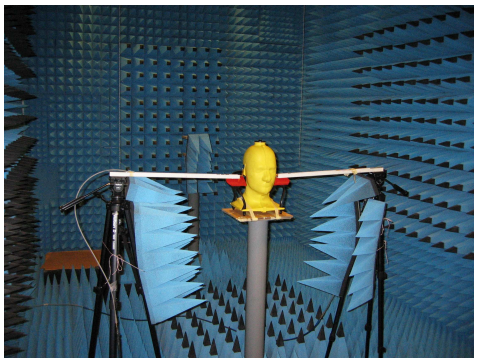

Fig. 1. Measurement setup with head phantom in the anechoic chamber

tissue simulation liquid HSL 5800, which consists of water, mineral oil, emulsifiers, additives and salt. This lossy dielectric liquid matches the requirements according to FCC [12] in the frequency range from 4.9 to 6.0 GHz. At 5.2 GHz relative permittivity is given by $\varepsilon_r = 36.0$ and conductivity by $\sigma = 4.66\frac{\mathrm{S}}{\mathrm{m}}$ and at 5.8 GHz by $\varepsilon_r = 35.3$ and by $\sigma = 5.27\frac{\mathrm{S}}{\mathrm{m}}$. As shown in Fig. 1 the head phantom was placed on a plastic pillar for the measurements.

III. Attenuation on the Head

In Fig. 2, frequency transfer functions are shown for different persons and the head phantom. It can be seen that transfer functions for all test persons are similar. The transfer function for the head phantom shows also a similar shape. But for a wide range of frequencies the attenuation is about 5-10dB smaller compared to the test persons. Although, the liquid in the head phantom is only specified for the frequency range from 4.9-6 GHz it seems to fit the attenuation characteristic of a human head over a wider frequency range. For comparison reasons, also the attenuation calculated with Friis Formula for an isotropic antenna and a reference measurement without head are shown in Fig. 2. It can be seen that the attenuation on the head is about 20-30 dB higher compared to the reference measurement and attenuation derived from Friis formula.

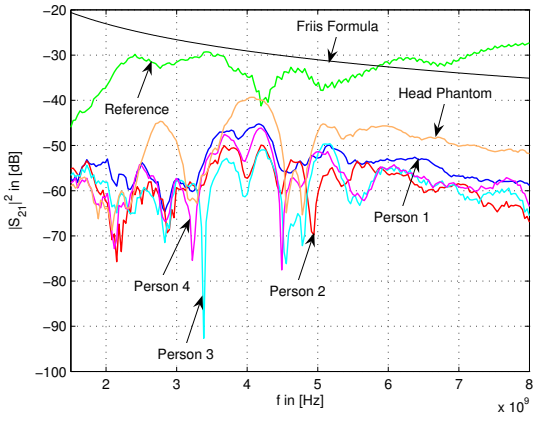

Fig. 2. Frequency transfer functions for different persons and head phantom

IV. Propagation Mechanisms

A. Direct Transmission through the Head

We start the propagation mechanism investigations by considering direct transmission through the head first. Wavelength and propagation speed of a wave are not the same for transmission through a lossy medium as for transmission through air. In a dielectric lossy medium, wavelength decreases and propagation speed is smaller compared to the speed of light [13]. Thus, the expected arrival time of a direct path through the head can be calculated from the wave's propagation speed through the head and from the distance between both antennas. Based on the permittivity and conductivity values given for the head phantom a direct path through the head would have an expected delay of

$$\Delta t = \frac{d}{v_{\text{head}}} - \frac{d}{c} = 2.92\text{ns} \qquad (1)$$

compared to the direct path of a reference measurement without head. In (1), $v_{\text{head}} = 4.88 \cdot 10^7 \frac{m}{s}$ denotes the propagation speed through the head, $c = 3 \cdot 10^8 \frac{m}{s}$ the speed of light, and $d = 0.17\text{m}$ the distance between both antennas.

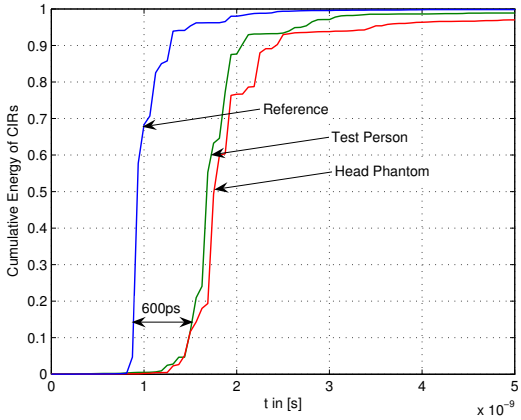

Fig. 3. Cumulative energy of channel impulse responses (CIRs) for transmission with and without head

In Fig. 3, cumulative energies of *channel impulse responses* (CIR) measured in an anechoic chamber with and without head are plotted. We assume the first paths of the CIRs at the time instances where the first significant increase of energy can be observed. It can be seen that the cumulative energy distributions are relatively similar for test person and head phantom. But the first paths of those CIRs are delayed by only about 600ps compared to the reference measurement. This delay of the first paths is much smaller than the calculated delay in (1). This difference between measured and calculated first paths leads to the assumption that there exist other propagation mechanisms for transmission on the head than direct transmission through the head. Since the cumulative energy plots for the head in Fig. 3 show no significant increase of energy at the expected delay from (1) we conclude that transmission through the head is negligible.

To verify the result that transmission through the head is negligible we calculate the attenuation for transmission

through the head. For this purpose, we consider the head as a lossy medium. Such a lossy medium can be described by its complex permittivity

$$\begin{aligned}\underline{\varepsilon}_r &= \varepsilon_r' - j\varepsilon_r'' \\ &= \varepsilon_r\left(1 - j\frac{\sigma}{\omega\varepsilon_0\varepsilon_r}\right) = \varepsilon_r\left(1 - jd_\varepsilon\right),\end{aligned} \tag{2}$$

with ε_r' and ε_r'' determining dispersion and losses respectively, and its complex permeability

$$\underline{\mu}_r = \mu_r' - j\mu_r'' = \mu_r\left(1 - jd_\mu\right) \tag{3}$$

where ε_r' and μ_r' correspond to the relative permittivity ε_r and the relative permeability μ_r of the lossless medium, respectively [13]. Using (2) and (3) the wave number

$$\underline{k} = k' - jk'' = \omega\sqrt{\varepsilon_0\underline{\varepsilon}_r\mu_0\underline{\mu}_r} \tag{4}$$

becomes complex. ε_0 and μ_0 denote permittivity and permeability in free space, respectively. Thus, the electrical field strength of a wave in a lossy medium as a function of the propagation distance z can be described by

$$\begin{aligned}E(z,t) &= \underline{E}\cdot e^{(j(\omega t - \underline{k}z))} \\ &= \underline{E}\cdot e^{k''z}\cdot e^{\left(j(\omega t - k'z)\right)},\end{aligned} \tag{5}$$

with the electric field-strength $\underline{E}$, the angular frequency $\omega = 2\pi f$, and time t. In (5), $e^{k''z}$ depicts the attenuation term containing

$$k'' = \frac{2\pi}{\lambda_\varepsilon}\cdot\Im\left\{\sqrt{1 - jd_\varepsilon}\right\}. \tag{6}$$

The wavelength λ_ε in a lossy dielectricum is given by

$$\lambda_\varepsilon = \frac{\lambda_0}{\sqrt{\varepsilon_r}\cdot\Re\left\{\sqrt{1 - jd_\varepsilon}\right\}}. \tag{7}$$

From (2) we get

$$d_\varepsilon = \frac{\sigma}{\omega\varepsilon_0\varepsilon_r}. \tag{8}$$

With $\lambda_0 = 0.06$m, which corresponds to a frequency $f_0 \approx 5.2$GHz, $\varepsilon_0 \approx \frac{10^{-9}}{36\pi}\frac{\text{As}}{\text{Vm}}$, $\mu_0 = 4\pi 10^{-7}\frac{\text{Vs}}{\text{Am}}$, $\mu_r \approx 1$ and using the relative permittivity and conductivity for the head phantom specified we get from (6)

$$k'' \approx -146.4\frac{1}{\text{m}}. \tag{9}$$

Putting this result in the attenuation term $e^{k''z}$ in (5) the attenuation for a distance of $z = 0.17m$, which corresponds to the distance between the antennas on the head, becomes

$$e^{k''z} = e^{-146.4\frac{1}{\text{m}}\cdot 0.17\text{m}} \approx -216.2\text{dB}. \tag{10}$$

Since relative permittivity and conductivity of the head phantom are very similar to human head tissues (cf. [14]), this result can be regarded also as valid for transmission through human heads. Calculations above show that the direct component of a transmission through the head is attenuated severely. This attenuation is much higher than expected from the transfer function plots in Fig. 2. Thus, we again conclude that energy transmitted through the head is negligible and that there have to exist other propagation mechanisms around the head, which cause the only slightly delayed transmission paths in Fig. 3.

B. Surface Waves

Since the human head consists of several layers of different tissues, surface waves are one possible propagation mechanism around the head. Surface waves travel along the boundary between two different media [13], also along curvatures. It is possible to measure surface waves by channel measurements with different distances between antennas and surface. If surface waves exist, the electromagnetic field decays exponentially moving the field detector away from the boundary between two tissues [15].

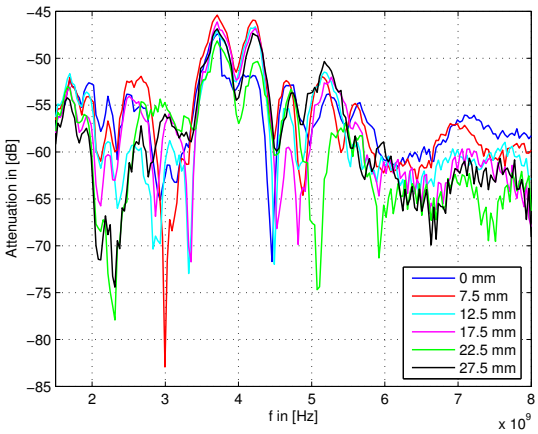

Fig. 4. Transfer functions for different distances between antennas and head surface

In Fig. 4, exemplary transfer functions on the head are shown for changing distances between both antennas and the skin. Since the transfer functions are plotted in logarithmic scale the attenuation should increase linearly with increasing distance if there exist surface waves around the head. The exponential decay of the field strength caused by surface waves is frequency dependent and can be calculated from the field component (cf. [15])

$$E_x \sim e^{-\Re\{u\}y}. \tag{11}$$

(11) can be solved by inserting the distance y between antenna and surface and

$$u = \sqrt{\frac{k_1^2 - k_2^2}{1 - \left(\frac{k_1^2}{k_2^2}\right)^2}} \tag{12}$$

with the squared wavenumber $k_1^2 = -j\omega\mu_0(\sigma + j\omega\varepsilon_0\varepsilon_r)$ and the squared wavenumber $k_2^2 = \omega^2\mu_0\varepsilon_0$ for air.

From (11), it can be seen that the field strength attenuation is increasing linearly in logarithmic scale with increasing distance. The slope of the field strength attenuation over distance becomes steeper with increasing frequency. This can be observed from Fig. 5 where the slopes of field strength attenuation are shown calculated from (11) with frequency dependent tissue values given in [14]. For the measurements, the slopes of the field strength attenuation are fitted for each frequency by using a least-square method. These approximated slopes of attenuation are also plotted in Fig. 5 and do not

exhibit an increase of the slope over distance with increasing frequency, which would be expected if surface waves would be dominant. For some frequencies even a decrease of attenuation with distance can be observed. Only for frequencies between 1.5 and 1.9 GHz calculated and measured decays of attenuation are in the same order of magnitude, i.e., no relevant surface waves can be detected in the frequency range between 1.9 and 8 GHz.

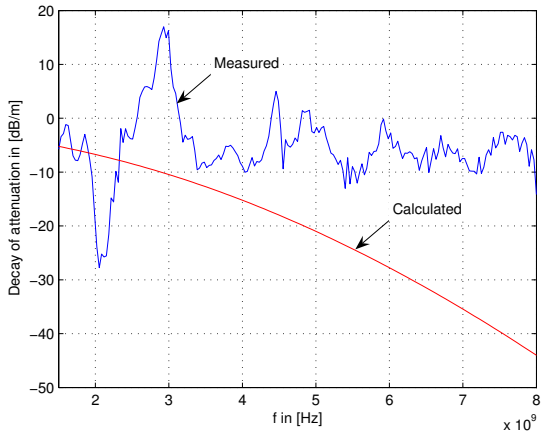

Fig. 5. Calculated and measured decays of attenuation

Moreover, surface waves are traveling with a speed slower than light speed [15] that also does not explain the slightly delayed first paths for the head measurement in Fig. 3. Thus, we conclude that surface waves are not the dominant propagation mechanism around the human body and that there has to exist some other dominant propagation mechanisms.

C. Reflection and Absorption

To verify if there exist any reflections or absorptions by the head, we measured the antenna pattern for the antenna mounted on the head phantom and compare it with the antenna pattern without head phantom. The antenna patterns were measured in the anechoic chamber with a VNA. The head with antenna and the antenna alone were mounted on a rotating table, respectively. The measurement setup is shown schematically in Fig. 6. Please note, that the antennas are not placed in the rotating axis since the center of the head is placed at this point.

Both antenna patterns are shown in Fig. 7. For the antenna pattern measurement with head phantom the antenna was mounted on the left ear as shown in Fig. 6. This antenna pattern is not symmetric since the antenna was not exactly placed on the position $\varphi = 270°$ and also the head itself is non-symmetric. At about $\varphi = 235°$ and $\varphi = 285°$ reflection effects can be seen, i.e., an attenuation decrease of about 3dB can be observed compared to the reference measurement. Similar to the observations in [7], attenuation of up to 23dB can be observed when the head is placed between the antennas. Especially, between $\varphi = 30°$ and $\varphi = 210°$ the head attenuates the signal. For this range of angles the head acts as obstacle between reference antenna and the antenna mounted on the head.

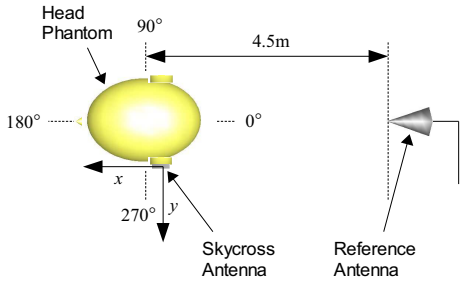

Fig. 6. Schematic measurement setup for antenna pattern measurements with head phantom (top view)

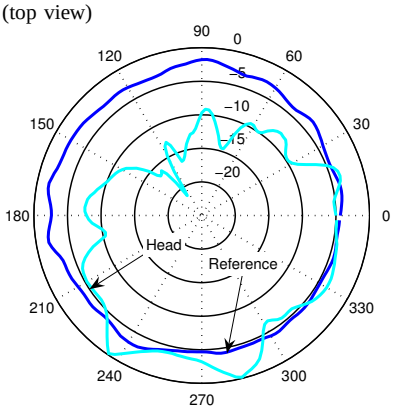

Fig. 7. Antenna pattern with antenna directly placed to the head and reference antenna pattern without head at $f = 3.125$ GHz

In Fig. 8, the forward reflection coefficient S_{11} is shown for an antenna directly mounted on the head. For comparison reasons the coefficient S_{11} is also depicted for a reference measurement without head. Only slight differences between reference and head measurement can be observed for frequencies below 3 GHz and above 6 GHz. Between 3 and 6 GHz the shapes of both curves are also similar, although variations of up to 10dB can be observed. Between 2.5 and 4.6 GHz the antenna match is even better if the antenna is mounted on the head compared to the reference, i.e., more power should be radiated by the antenna. From the observation in Fig. 7 that reflections from the head can be seen only under certain directions and from the results in Fig. 8 we conclude that the head is absorbing most energy that is transmitted into its direction. We conclude that reflection and absorbtion effects are existing on the human head. But for the envisioned propagation scenario from one side of the head to the opposite, reflection and absorption play only a subsidiary role.

D. Diffraction

It was shown in the sections above that neither direct transmission nor surface waves are the dominant propagation mechanisms on the human head. Although, reflections of the human head can be observed this propagation mechanism can be neglected for transmission from one side of the head to the opposite. Thus, diffraction remains as possible candidate. If the direct path between transmitter and receiver is obstructed by an obstacle, waves can travel into the shadow zone behind the obstacle. Such a kind of diffraction is then also called

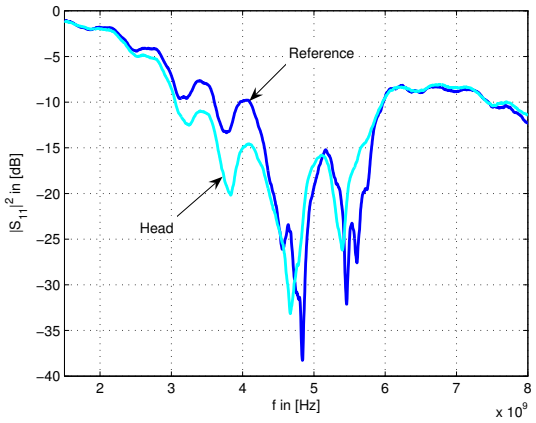

Fig. 8. S_{11} Parameter for an antenna directly placed on the head and for an antenna without head as reference

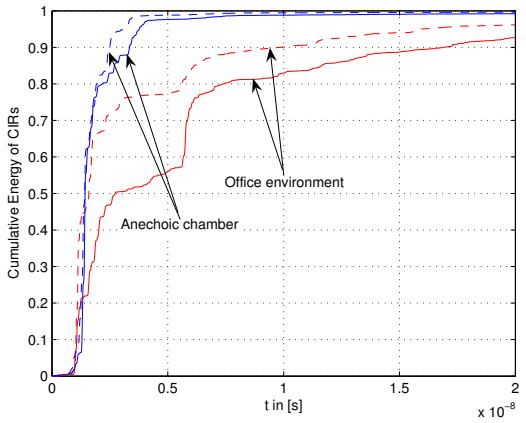

Fig. 9. Cumulative energy of channel impulse responses in office environment and anechoic chamber; the antenna's main directivity was changed from horizontal backward (dashed lines) to vertical to the floor (solid lines)

"creeping" waves [16]. However, diffraction effects are only relevant if the obstacle dimensions are not greater than about 60 times the wavelength [17]. This is fulfilled in our case where the wavelengths remain above about $\lambda = 3$cm. Since diffracted waves travel with speed of light, the additional path length compared to the reference path length can be calculated from the time delays in Fig. 3. There, it can be observed that the first paths for transmission on the head are delayed by about 600ps compared to the reference path. Such delay corresponds to a way that is about

$$\Delta z = 600 \cdot 10^{-12}\text{s} \cdot 3 \cdot 10^{8} \frac{\text{m}}{\text{s}} = 0.18\text{m} \qquad (13)$$

longer than the direct path of $z \approx 0.17$m. The increased path length corresponds with the distance between both ears on the head surface. This indicates that diffraction is probably the dominant propagation mechanism.

If we consider the head as circular cylinder for simplicity, equations given in [18] can be used to determine the field in the shadow region caused by one ray and hence the attenuation of a diffracted wave around the cylinder. For both antennas directly placed on the cylinder surface the field is approximated depending on the angle φ by

$$H(\varphi) \approx -q \cdot e^{-jka} \int_{-\infty}^{\infty} \frac{w_2(\tau)}{w_2'(\tau)} e^{-j\xi\tau} d\tau. \qquad (14)$$

k denotes the wave number, a the distance between both antennas on the cylinder surface, and $w_2(\tau) = \sqrt{\pi}(Bi(\tau) - jAi(\tau))$ the Fock-type Airy function. ξ depends on the angle between both antennas, the wave number, and the cylinder radius. q depends on the angle between both antennas, the radius of the cylinder, the source strength, the wave number, and the frequency f. A detailed description on the parameters in (14) can be found in [18]. Inserting conductivity and permittivity values from [14] for brain tissue into (14) and averaging over N_f frequencies f, an attenuation of

$$D = \frac{1}{N_f} \sum_{f=1.5GHz}^{8GHz} \left(|H(\varphi \approx 0)|^2 - |H(\varphi = \pi)|^2 \right) \approx 60\text{dB} \qquad (15)$$

can be calculated for antennas placed on opposite sides of the cylinder. The attenuation calculated in (15) corresponds approximately with the measured attenuation in Fig. 2. Of course, it does not exist only one ray and thus also constructive and destructive interference may occur. But since path delays correspond very well with increased distances on the head surface, since both measurements and calculation show attenuation of same order of magnitude and since other propagation mechanisms can be excluded as described above, we conclude that diffraction is the dominant propagation mechanism around the head.

V. Impact of Propagation Mechanisms on a BAN Communication System

The presented propagation results have direct impact on the design of a BAN communication system.

As shown in [19] and [20], performance of *transmitted reference* (TR) receiver and *energy detector* (ED) strongly depend on the integration time used in such receivers. In Fig. 9 cumulative energies of CIRs are plotted for anechoic chamber and office environment. Dashed lines depict measurements where the antennas' main directivity pointed towards the floor. For the measurements depicted by solid lines the antennas were rotated such that their main directivity pointed backwards. It can be observed for the anechoic chamber CIRs that almost the whole energy is contained in a window of about only 3.5ns, i.e., the integration length is very small for an ED or TR receiver. Compared to the channel measured in the anechoic chamber energy can also be captured from multipath reflections in the office environment. In Fig. 9, especially a path at about 6ns is obvious. This path is caused by a table, the test person was sitting in front of. For the backward orientation of the antenna this path is not as strong due to the above mentioned directivity of the antenna. Nevertheless, first paths around the head caused by diffraction can also be observed in the office environment. Using the 3.5ns window size determined from the anechoic chamber measurements it is possible to collect about 50 and 75 % of the whole energy in the office environment, respectively, as shown in Fig. 9.

This means that the receiver is insensitive to environment changes by choosing a very short integration length, i.e., by only collecting energy of paths diffracting around the head.

Of course, an adaptive receiver, which adapts its integration length according to the environment, could achieve better performance. But due to complexity reasons, an ED or TR receiver with fixed integration length is favorable for the use in BANs.

It was shown that direct transmission through the head is negligible and that diffraction is the main propagation mechanism around the head. This has also strong impact on the design of antennas used in wireless BAN. Antennas should be designed such that almost the whole energy is radiated along the head surface to take advantage of diffraction and neither into the head nor away from the head. With such an antenna the energy that can be collected from reflections will be reduced. But this will not influence performance of a ED or TR receiver with fixed short integration length that only collects energy from paths around the head as described above. Using antennas that do not radiate away from the head does not only reduce the energy that can be collected from reflections but also reduces interference caused by other wireless systems in close vicinity that might prohibit UWB communication [21]. Since the surface of the human body looks like a plane for small areas only and usually exhibits curvatures, also dipoles mounted perpendicular to the body surface are suited for the use in BANs. For such mounting of a dipole, energy is radiated along possible curvatures on the body but not directly into the body due to the dipole characteristic.

If energy shall be collected from reflections using an ED or TR receiver with adaptive integration length, antennas isotropically radiating into a half-space away from the head can be used. One antenna type fulfilling such a requirement approximately is the monopole [22].

VI. Conclusions

In this paper we investigated the main propagation mechanisms on the human head. We showed by means of measurements and theoretically that direct transmission can be neglected for transmission from one side of the head to the opposite. Moreover, it could be observed that surface waves are also not the dominant propagation mechanisms. Although, reflections and absorptions could be observed these mechanisms are not dominant for transmission from one side of the head to the opposite. Based on the results above we concluded that diffraction is the dominant propagation mechanism around the head. This result corresponds with the FDTD (Finite Difference Time Domain) simulation results for transmission on the torso in [10]. From simulations, the authors also did not observe a direct path through the torso and assumed that waves are rather diffracting around the torso. Since most energy transmitted into the head is absorbed by the tissue we concluded that antennas should be designed such that they take advantage of diffraction. Additionally, it was shown that ED and TR receiver with fixed short integration length are independent of the environment and therefore well suited for the use in wireless BANs.

References

[1] P. Coronel, W. Schott, K. Schwieger, E. Zimmermann, T. Zasowski, H. Maass, I. Oppermann, M. Ran, and P. Chevillat, "Wireless body area and sensor networks," *Wireless World Research Forum (WWRF) Briefings*, December 2004.

[2] N. B. Bharatula, S. Ossevoort, M. Stäger, and G. Tröster, "Towards wearable autonomous microsystems," *Pervasive Computing: Proceedings of the 2nd Int'l Conference*, pp. 225–237, April 2004.

[3] J. Bernhard, P. Nagel, J. Hupp, W. Strauss, and T. von der Grün, "BAN - body area network for wearable computing," *9th Wireless World Research Forum (WWRF)*, July 2003.

[4] S. Jung, C. Lauterbach, M. Strasser, and W. Weber, "Enabling technologies for disappearing electronics in smart textiles," *2003 IEEE ISSCC*, vol. 1, pp. 386–387, February 2003.

[5] D. Porcino and W. Hirt, "Ultra-wideband radio technology: Potential and challenges ahead," *IEEE Communications Magazine, Vol. 41, No. 7*, pp. 66–74, July 2003.

[6] D. Barras, F. Ellinger, and H. Jäckel, "A comparison between ultra-wideband and narrowband transceivers," in *IEEE Wireless 2002*, 2002.

[7] T. B. Welch, R. L. Musselman, B. A. Emessiene, P. D. Gift, D. K. Choudhury, D. N. Cassadine, and S. M. Yano, "The effects of the human body on UWB signal propagation in an indoor environment," in *IEEE Journal on Selected Areas in Communications, Vol. 20, No. 9*, December 2002.

[8] T. Zasowski, F. Althaus, M. Stäger, A. Wittneben, and G. Tröster, "UWB for noninvasive wireless body area networks: Channel measurements and results," *IEEE UWBST 2003*, November 2003.

[9] I. Z. Kovács, G. F. Pedersen, P. C. F. Eggers, and K. Olesen, "Ultra wideband radio propagation in body area network scenarios," *IEEE ISSSTA 2004*, pp. 102–106, September 2004.

[10] A. Fort, J. Ryckaert, C. Desset, and S. Donnay, "Ultra wide-band body area channel model," *12th Wireless World Research Forum (WWRF)*, November 2004.

[11] Schmid & Partner Engineering AG, SPEAG, Zurich, Switzerland, http://www.speag.com.

[12] D. L. Means and K. W. Chan, "Evaluating compliance with FCC guidelines for human exposure to radiofrequency electromagentic fields, additional information for evaluating compliance of mobile and portable devices with FCC limits for human exposure to radiofrequency emissions," *FCC Supplement C (Edition 01-01) to OET Bulletin 65 (Edition 97-01)*, pp. 1–53, June 2001.

[13] H. Meinke and F. W. Gundlach, *Taschenbuch der Hochfrequenztechnik, Band 1*, 5th ed. Springer-Verlag, 1992.

[14] FCC, "Tissue dielectric properties calculator," *http://www.fcc.gov/fcc-bin/dielec.sh, based on results from "Compilation of the Dielectric Properties of Body Tissues at RF and Microwave Frequencies" by Camelia Gabriel, Brooks Air Force Technical Report AL/OE-TR-1996-0037*.

[15] H. M. Barlow and J. Brown, *Radio Surface Waves*. Oxford University Press, 1962.

[16] L. B. Felsen and N. Marcuvitz, *Radiation and Scattering of Waves*, 10th ed. IEEE Press Series on Electromagnetic Waves, 1994.

[17] R. Schmitt, *Electromagnetics Explained, A Handbook for wireless/RF, EMC, and High-speed Electronics*, 10th ed. Newnes, Elsevier Science, 2002.

[18] R. Paknys, "Uniform asymptotic formulas for the creeping wave field on or off a cylinder," *IEEE Trans. on Antennas and Propagation, Vol. 41, No. 8*, vol. 41, pp. 1099–1104, August 1993.

[19] T. Zasowski, F. Althaus, and A. Wittneben, "An energy efficient transmitted-reference scheme for ultra wideband communications," *Joint UWBST & IWUWBS 2004*, May 2004.

[20] M. Weisenhorn and W. Hirt, "Robust noncoherent receiver exploiting UWB channel properties," *Joint UWBST & IWUWBS 2004*, May 2004.

[21] T. Zasowski, F. Althaus, and A. Wittneben, "Temporal cognitive UWB medium access in the presence of multiple strong signal interferers," *14th IST Mobile & Wireless Communications Summit*, June 2005.

[22] I. Hickman, *Practical Radio-Frequency Handbook*, 3rd ed. Newnes, Elsevier Science, 2002.